Analytical Biochemistry 421 (2012) 213–218

Contents lists available at SciVerse ScienceDirect

Analytical Biochemistry

journal homepage: www.elsevier.com/locate/yabio

Size-dependent plasmonic responses of single gold nanoparticles for analysis of biorecognition

Woo Sung Hwang [a], Phuoc Long Truong [a], Sang Jun Sim [b,*]

[a] Department of Chemical Engineering, Sungkyunkwan University, Suwon 440-746, Republic of Korea
[b] Department of Chemical and Biological Engineering, Korea University, Seoul 136-713, Republic of Korea

ARTICLE INFO

Article history:
Received 4 August 2011
Received in revised form 8 October 2011
Accepted 2 November 2011
Available online 12 November 2011

Keywords:
Localized surface plasmon resonance (LSPR)
Gold nanoparticle (AuNP)
Biomolecular recognition
Resonant Rayleigh light scattering

ABSTRACT

We report the use of plasmonic responses of single gold nanoparticles (AuNPs) with various sizes for the analysis of biomolecular recognition. We also describe the relationship between particle size and plasmonic response induced by the binding of receptors and target analytes. To investigate the plasmonic response of AuNPs, Rayleigh light scattering spectra were collected from individual AuNPs using a dark-field microspectroscopy system. Using prostate-specific antigen (PSA) as a model, the linear dynamic range was obtained in the concentration range of 10^{-4} to 10 ng/ml, with the smallest detectable concentration at 0.1 pg/ml corresponding to localized surface plasmon resonance (LSPR) λ_{max} shifts of approximately 2.95 nm. This result indicates that individual AuNPs can be used for development of a very sensitive, robust, simple, and label-free biosensor to detect protein biomarkers. Furthermore, the method possesses great potential for monitoring other biological interactions.

Greater understanding of nanoscience and nanoscale phenomena is essential for the development of devices based on nanotechnology. In particular, the optical properties of nanostructures have been the subject of intensive research efforts owing to their applications in research fields such as surface-enhanced spectroscopies [1–3], second harmonic generation [4–7], and surface plasmonic amplifiers [8]. Above all, as one of the devices based on the optical properties of metal nanostructure, localized surface plasmon resonance (LSPR)[1] biosensors have recently attracted considerable attention [9–13].

LSPR is a phenomenon caused by the collective oscillation of conductive free electrons on the surface of noble metal nanostructures owing to the excitation of the electromagnetic field of the incident light and is manifested by a peak in the extinctive spectrum of the nanostructures. The results of excitation are selective photon absorption, strong light scattering, and local electromagnetic field enhancement. This phenomenon does not occur in the spectrum of the bulk metal and is responsible for wavelength selective absorption with extremely large molar extinction coefficients of approximately $3.0 \times 10^{11}\ M^{-1}\ cm^{-1}$ and resonant Rayleigh light scattering with an efficiency equivalent to that of 10^6 fluorophores [14,15]. Moreover, the wavelength of the LSPR peak is strongly dependent on size, shape, composition, and interparticle spacing of the nanoparticle as well as on local dielectric environment [16–23].

The advent of dark-field microscopy has enabled the study of the optical properties of single metal nanoparticles. By coupling a dark-field microscope to an imaging monochromator and a highly sensitive charge-coupled device (CCD) camera, the Rayleigh light scattering spectra from single metal nanoparticles can be measured easily [24]. The scattering signal of single nanoparticles obtained on the dark-field microspectroscopy system has the advantage of a high signal-to-noise ratio owing to the measurements in the presence of a very low background [15]. Furthermore, the scattering spectrum of single nanoparticles exhibits homogeneous sharpening compared with the ensemble spectrum, and these spectral features make it possible to provide more accurate determination of peak shifts [25].

In previous studies, we reported the proof of concept of using the resonant Rayleigh light scattering spectra of individual gold nanoparticles (AuNPs) for analysis of antigen–antibody recognition [26,27]. Currently, nanorods are proven to have more advantages compared with nanospheres owing to their higher sensitivity to

* Corresponding author. Fax: +82 2 926 6102.
E-mail address: simsj@korea.ac.kr (S.J. Sim).

[1] *Abbreviations used:* LSPR, localized surface plasmon resonance; CCD, charge-coupled device; AuNP, gold nanoparticle; PSA, prostate-specific antigen; ACT, α_1-antichymotrypsin; mAb, monoclonal antibody; BSA, bovine serum albumin; IgG, immunoglobulin G; $HAuCl_4{\cdot}3H_2O$, hydrogen tetrachloroaurate(III) trihydrate; $NH_2OH{\cdot}HCl$, hydroxylamine hydrochloride; NHS, *N*-hydroxysuccinimide; EDC, *N*-ethyl-*N*-(3-diethylaminopropyl) carbodiimide; PBS buffer, phosphate-buffered saline in foil pouches; OEG_6–COOH, $HS(CH_2)_{11}(OCH_2CH_2)_6OCH_2COOH$; HR–TEM, high-resolution transmission electron microscopy; FE–SEM, field emission scanning electron microscopy; DI, deionized.

0003-2697/$ - see front matter © 2011 Elsevier Inc. All rights reserved.
doi:10.1016/j.ab.2011.11.001

refractive index changes, distinct optical properties, and clear LSPR spectral shifts [27]. However, nanospheres, which can be either obtained from the commercial sources with various sizes or conveniently produced in laboratories, are still popular and used for biomedical applications due to their high chemical stability, convenient surface bioconjugation with antibodies and DNA probes, and unique optical properties [28–31]. In this study, we systematically investigated the plasmonic responses of single AuNPs with various sizes for a comparative analysis of the LSPR behavior induced by the binding receptors and target analytes on the surface of each AuNP. Moreover, the linear dynamic range of the plasmonic response of each AuNP was examined to demonstrate possibilities for use of single AuNPs with various sizes as a biosensor. Consequently, the total linear dynamic range for prostate-specific antigen and α_1-antichymotrypsin (PSA–ACT complex) detection could be obtained at a concentration range of 10^{-4} to 10 ng/ml, and the smallest concentration at 0.1 pg/ml could be detected with a small LSPR λ_{max} shift of approximately 2.95 nm. The results show that this study can be used for fabrication of a label-free biosensor, allowing quantitative analysis of cancer-associated proteins in a wide concentration range, and also can be expanded to design other biomolecular binding assays.

Materials and methods

Chemicals and materials

Human PSA–ACT complex and PSA–ACT complex monoclonal antibody (PSA–ACT mAb) were supplied by BiosPacific (Emeryville, CA, USA). Bovine serum albumin (BSA), human immunoglobulin G (IgG), fibrinogen from human plasma, hydrogen tetrachloroaurate(III) trihydrate ($HAuCl_4{\cdot}3H_2O$, 99.9%), hydroxylamine hydrochloride ($NH_2OH{\cdot}HCl$), sodium citrate, absolute ethanol, ethanolamine, *N*-hydroxysuccinimide (NHS), *N*-ethyl-*N*-(3-diethylaminopropyl) carbodiimide (EDC), and phosphate-buffered saline in foil pouches (PBS buffer, pH 7.4) were purchased from Sigma–Aldrich (Korea). $HS(CH_2)_{11}(OCH_2CH_2)_6OCH_2COOH$ (OEG_6–COOH) was purchased from Cos Biotech (Korea). A coverslip slide ($22 \times 40 \times 0.1$ mm) was purchased from Deckglaser (Germany). Ultrapure water (18.2 mΩ cm^{-1}) was used to prepare all chemical solutions.

Synthesis of AuNPs

Spherical AuNPs with various sizes were prepared by hydroxylamine reduction coupled with a seed-mediated growth procedure [32]. Briefly, all glassware was thoroughly cleaned with aqua regia (3:1 HNO_3/HCl) and rinsed extensively with ultrapure water (18.2 mΩ cm^{-1}). Next, to prepare the Au seeds, 5.0 ml of 1% sodium citrate, 1.7 ml of 1% $HAuCl_4$ solution, and 50 ml of fresh water were quickly mixed with heating and stirring in a round-bottom flask. The mixture was then refluxed for 15 min and cooled down to room temperature with continuous stirring. Subsequently, the suspension was filtered using a 0.22-μm filter to remove any aggregated particles. After synthesis of the Au seeds, the suspension was used to prepare larger sized AuNPs. The AuNPs with different diameters were synthesized by adjusting the volume of the Au seeds added to a solution with 0.5 ml of 1% $HAuCl_4$, 2.1 ml of 40 mM $NH_2OH{\cdot}HCl$, and 95 ml of H_2O. This reaction was carried out at room temperature. The size and morphology of the synthesized AuNPs were estimated by high-resolution transmission electron microscopy (HR–TEM, JEOL JEM-3011 operated at 300 kV), and the dispersity of the AuNPs immobilized onto the glass surface was observed by field emission scanning electron microscopy (FE–SEM, JEOL JSM6700F operated at 15 kV).

Sample preparation

To investigate the optical response of individual nanoparticles, all AuNP solutions were diluted with ultrapure water to an optical density of 0.2 at 520 nm. Next, the AuNPs were immobilized by drop-coating onto a coverslip slide for 4 to 6 h at room temperature. Subsequently, the glass slide was mounted onto an RC-30 closed-bath imaging chamber (Warner Instruments, Holliston, MA, USA) to visualize the AuNPs as well as to investigate the LSPR response of single nanoparticles induced by the adsorbates and reactants. Afterward, the chamber was inserted onto the sample holder of the dark-field microscope and a fluidic flow was settled by connecting with a syringe pump (Harvard Apparatus, Holliston, MA, USA).

Dark-field microspectroscopy

To observe the scattered light of single metal nanoparticles, a transmission configuration for the resonant Rayleigh light scattering microspectroscopy was established using a dark-field microscope (Eclipse TE2000-U, Nikon) (Fig. 1). For spectral measurements, the microscope was equipped with a spectrograph (Microspec 2300i, Roper Scientifics, Sarasota, FL, USA) and a CCD camera (PIXIS: 400B, Princeton Instruments, Trenton, NJ, USA). A color camera (D50, Nikon) was mounted on the front port of the microscope. A 100-W tungsten lamp and a dark-field condenser (dry condenser, NA = 0.80–0.95, Nikon) were used to illuminate the nanoparticles. The scattered light was collected with a 100× objective (CFI Plan Fluor ELWD, NA = 0.6) and directed to the spectrograph to be dispersed into monochromatic light. The CCD camera was used to measure the intensity of the monochromatic light, which was recorded as a function of light scattering intensity versus wavelength.

LSPR response investigation of individual AuNP sensors induced by adsorbates and target analytes (PSA–ACT complex)

For the LSPR response investigation of individual AuNPs, the first step was to functionalize the surface of individual AuNPs. The experimental process was carried out as follows (Fig. 1). First, the surface of AuNPs was cleaned by injecting an absolute ethanol solution for 10 min and then was washed with deionized (DI) water for 5 min to remove all contaminants and unbound AuNPs. Because the AuNPs were electrostatically immobilized onto the glass surface, a further normalizing step was performed by injecting DI water for another 30 min to remove any free AuNPs from the chamber. Next, the thiol derivative OEG_6–COOH was used to functionalize the particle surface before being chemically capped with the capture antibody. Briefly, 1.0 ml of an absolute ethanol solution containing 0.4 mM OEG_6–COOH was injected over the immobilized AuNPs, followed by an incubation period of 10 h. The carboxyl groups of OEG_6–COOH were subsequently activated by injecting 2.0 ml of a mixed solution of 0.1 M NHS and EDC for 10 min. Next, PSA–ACT mAb was immobilized onto the surface of AuNPs by injecting 1.0 ml of PSA–ACT mAb (10.0 μg/ml) and incubating for 2 h. Subsequently, 1.0 ml of 0.2 M ethanolamine was injected over the flow cell to deactivate the unreacted sites on the surface of the AuNPs and was incubated for 30 min. After the immobilization of PSA–ACT mAb, human PSA–ACT complex with various concentrations ranging from 0 to 10^2 ng/ml diluted in PBS buffer (pH 7.4) was injected over the surface of AuNPs and incubated for 1 h. At each step of the chemical binding, the sensor surface was rinsed by injecting DI water over the flow cell for 5 min, and the LSPR λ_{max} shift induced by the binding of analytes was recorded by measuring the scattering spectrum of individual AuNPs in DI water. Due to the fluctuation of the Rayleigh light scattering spectrum, the

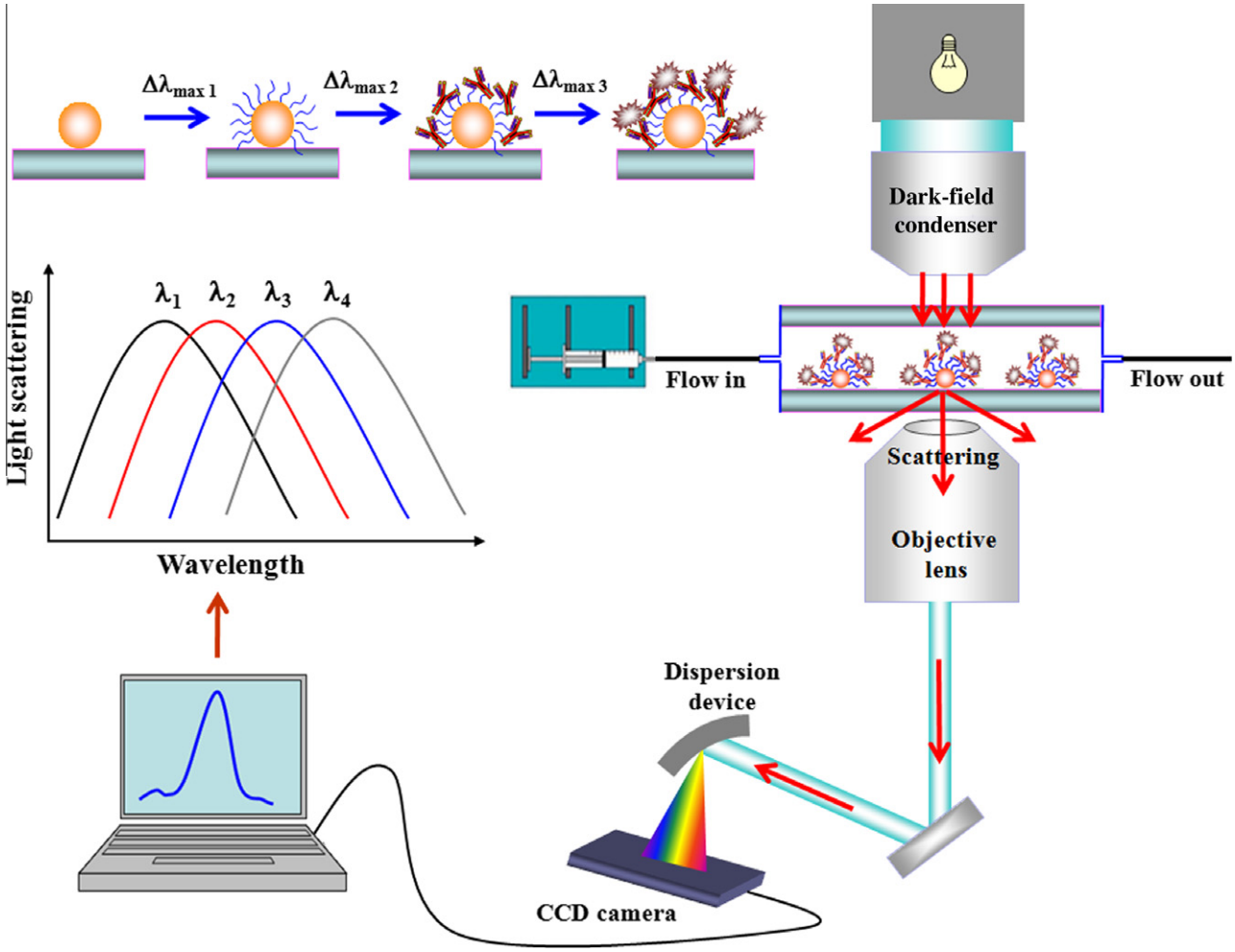

Fig.1. Scheme for the system setup using an inverted dark-field microscope and overall procedure describing the experimental processes.

Lorentzian algorithm was applied to fit the spectrum. OriginPro 7.5 software was used to provide accurate and efficient peaks as well as to remove the noise. The LSPR λ_{max} shift was calculated as follows: $\Delta\lambda_{max} = \lambda_{max}$ (after chemical binding) $- \lambda_{max}$ (before chemical binding).

For data collection, spectral signatures from many single AuNPs selected in the field of view were first identified. Subsequently, the optical responses of the same set of the specified AuNPs induced by the binding of adsorbates were systematically recorded as the spectral changes corresponding to the binding of adsorbates and target analytes. The data collected from every step of adsorption completed the statistical analysis and the error propagation during the calculation.

Results and discussion

AuNPs were chosen as plasmonic transducers of binding events for the following reasons. First, gold was chosen over silver, even though silver particles exhibit a higher local refractive index sensitivity than gold particles of the same shape and size [33], because the greater reactivity of silver compared with gold makes it less suitable for use in biologically relevant devices. Second, AuNPs are nontoxic and nonradioactive, making them ideal platforms for quantification of biochemical species and monitoring of dynamic processes inside biological cells [34].

For preparation of homogeneous samples, AuNPs with various sizes were synthesized through hydroxylamine reduction coupled with seed-mediated growth (the details of the synthesis were described in Materials and methods). The size and morphology of AuNPs were estimated by HR–TEM. The sizes of AuNPs were determined as mean values from counting three to five representative regions within each image. As a result, the average diameters of 21.1 ± 1.9, 42.9 ± 4.1, and 81.2 ± 6.2 nm were obtained from three synthesized AuNP samples. Fig. 2A shows the TEM image of the spherical AuNPs with an average diameter of approximately 21 nm, and the dispersion of the AuNPs that were immobilized onto the glass surface was observed by FE–SEM (Fig. 2B). As shown in Fig. 2B, the AuNPs were randomly arranged on the glass surface, and the arrangement state of the AuNPs observed by FE–SEM was in both individually isolated and aggregated forms. To reduce interparticle coupling effects, only individual nanoparticles with a particle-to-particle spacing of approximately greater than 2.5 times the particle diameter were selected for investigation because it has been indicated that the plasmon resonance peaks were remarkably shifted to the longer wavelength area when the interparticle spacing was reduced [35,36]. Thus, the AuNP solution was diluted with ultrapure water to an optical density of 0.2 at 520 nm prior to the immobilization of the AuNPs on the glass slide.

Using a dark-field microscope, the individual AuNPs immobilized on the glass slide could be visualized with the naked eye in the field of view as the bright spots with ultralow background scattering from the glass substrate (Fig. 2C). White light from a 100-W tungsten lamp was focused under large angles onto the sample using a dark-field condenser. The scattered light of a single AuNP

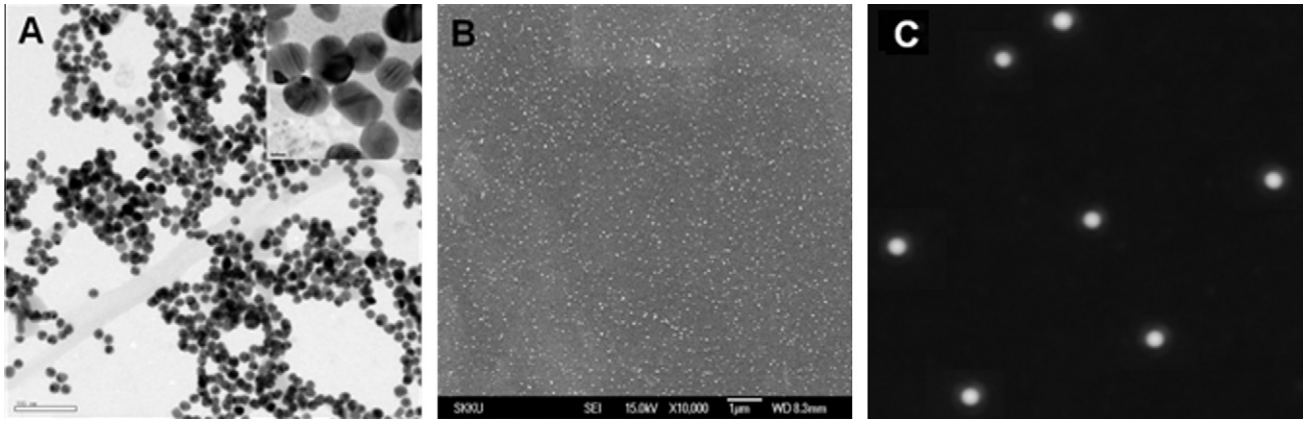

Fig.2. (A) HR–TEM images of AuNPs with an average diameter of approximately 21 nm (inset: image of AuNPs at higher magnification). (B) FE–SEM image of AuNPs immobilized on the glass slide. (C) Dark-field image of AuNPs immobilized on the glass surface at a magnification of 1500×.

in focus could be collected by a 100× objective lens, spectrally resolved in a grating spectrograph, and detected with a highly sensitive CCD camera. The position of every single nanoparticle could be located easily by adjusting the sample stage and microslit. The background spectrum was measured in an adjacent position to the individual AuNPs, and the noise caused by the instrumentation itself was excluded from the presented light scattering spectrum.

For measuring the Rayleigh scattering spectra of single AuNPs, the AuNPs were immobilized on a glass slide to observe their optical response. It is well known that the LSPR of noble metal nanoparticles is strongly dependent on their size, shape, and local dielectric environment. Hence, it is necessary to investigate the plasmonic response of AuNPs with various sizes for a comparative analysis of their LSPR behavior at the single nanoparticle level. In the case of the AuNPs with a diameter of approximately 21 nm, the LSPR λ_{max} values were obtained in a wavelength range of 558.95 to 574.5 nm. However, in the case of the AuNPs with approximate diameters of 43 and 81 nm, the LSPR λ_{max} values were obtained in wavelength ranges of 566.1 to 579.81 nm and 575.1 to 585.61 nm, respectively. These results show the size dependence of resonant Rayleigh light scattering spectra of the single AuNPs. A spectral position experiences a polaritonic red shift with increasing particle size owing to electromagnetic retardation [28,37]. Fig. 3A shows the representative resonant Rayleigh light scattering spectra of the individual AuNPs with an approximate diameter of 21 nm collected after every adsorption of the chemical molecules. The experimental spectra were fitted by the Lorentzian algorithm, and the λ_{max} shifted to the longer wavelength area for every step of adsorption. The LSPR λ_{max} shifts were approximately 15.07, 29.93, and 44.08 nm for formation of a self-assembled monolayer (SAM) of OEG_6-COOH, adsorption of PSA–ACT mAb, and PSA–ACT complex (0.1 ng/ml), respectively, compared with the LSPR λ_{max} of bare AuNPs. Afterward, the experiment was further expanded to the detection of the PSA–ACT complex at concentrations ranging from 10^{-5} to 10^{2} ng/ml. We also investigated the plasmonic response of single AuNPs with various sizes in the same conditions. As shown in Fig. 3B, the saturation response of the individual AuNP sensor was dependent on size of AuNPs. In the case of the AuNPs with a diameter of approximately 21 nm, the saturated concentration was 0.1 ng/ml. On the other hand, in the case of the AuNPs with approximate diameters of 43 and 81 nm, the saturated concentrations were 1.0 and 10 ng/ml, respectively. The saturation response of the individual AuNP sensor could be explained due to an overload of protein stacked onto the surface of AuNPs. These results also indicated that the maximum number of protein molecules conjugated to the surface of AuNPs was dependent on particle size [15,26].

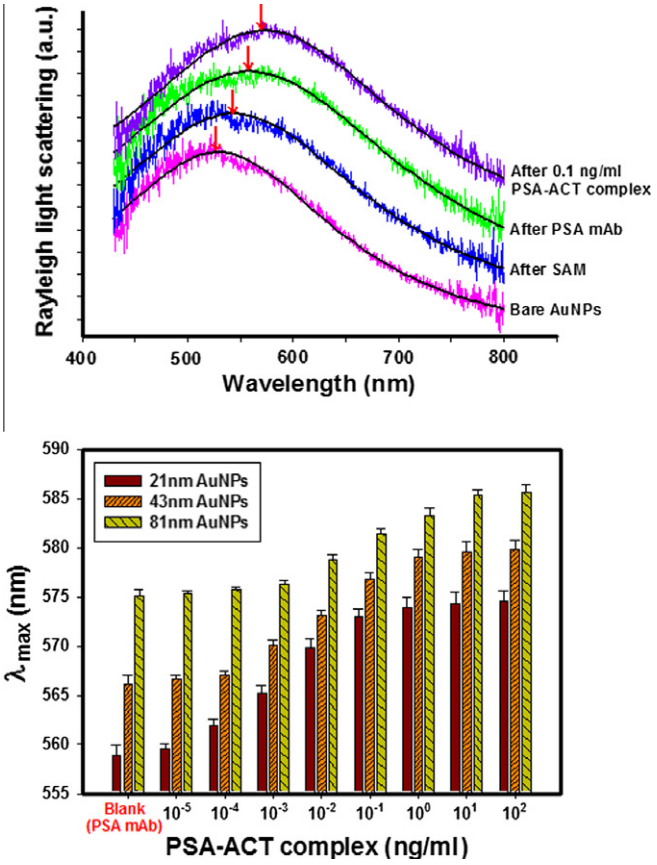

Fig.3. (A) Representative Rayleigh light scattering spectra of single AuNPs with a diameter of approximately 21 nm fitted to a Lorentzian algorithm. LSPR λ_{max} values are shifted to the longer wavelengths after every step of chemical binding of adsorbates and target analytes. a.u., arbitrary units. (B) LSPR λ_{max} values of each single AuNP with different sizes corresponding to the binding of the PSA–ACT complex with concentrations ranging from 10^{-5} to 10^{2} ng/ml. The LSPR λ_{max} values of each blank signal represent plasmonic responses obtained by the adsorption of PSA mAb (10 μg/ml) prior to binding of the PSA–ACT complex. The error bars illustrate the relative standard deviation for four replicates.

The calibration curves for the PSA–ACT complex detection using the single AuNPs as a biosensor are shown in Fig. 4. The plots show that the LSPR λ_{max} shift values of single AuNPs decrease with increasing size of AuNPs. This result indicates that changes in the refractive index surrounding the nanoenvironment of smaller

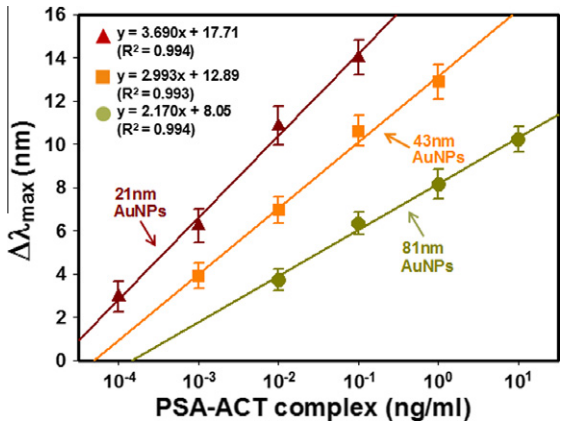

Fig.4. Calibration curves describing detection of the PSA–ACT complex at concentrations ranging from 10^{-4} to 10^{1} ng/ml using individual AuNPs with different sizes.

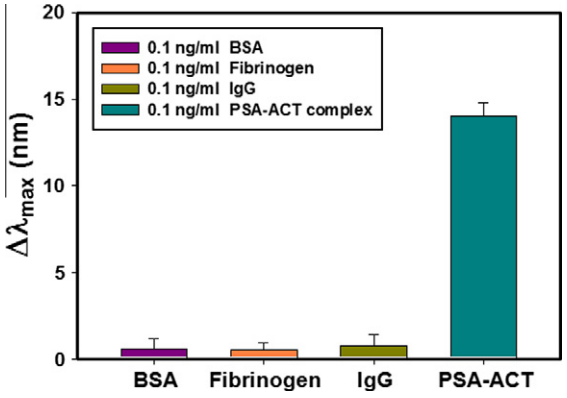

Fig.5. Nonspecific binding of various proteins on the anti-PSA functionalized AuNP surface (diameter = 21 nm). The LSPR peak shifts increased negligibly when 0.1-ng/ml concentrations of BSA, IgG, and fibrinogen were injected over the anti-PSA functionalized AuNP surface in the flow cell.

AuNPs are relatively larger when analytes of similar amounts are conjugated to the surface of AuNPs. Thus, as shown in Fig. 3B, in the case of AuNPs with diameters approximately 43 and 81 nm, the concentrations of analytes below 1.0 and 10 pg/ml, respectively, could not be determined. The lowest concentration that an individual AuNP sensor with a diameter of approximately 21 nm could experimentally detect was 0.1 pg/ml, corresponding to an LSPR λ_{max} shift of approximately 2.95 nm. Fig. 4 shows the linear scale of the plasmonic responses of single AuNPs with different sizes. The linear regression equations of each plasmonic response of a given size for PSA–ACT complex detection by a PSA–ACT complex/PSA–ACT mAb interaction were as follows: $y = 3.690x + 17.71$ ($R^2 = 0.994$, $n = 4$, diameter = 21 nm AuNPs), $y = 2.993x + 12.89$ ($R^2 = 0.993$, $n = 4$, diameter = 43 nm AuNPs), and $y = 2.170x + 8.05$ ($R^2 = 0.994$, $n = 4$, diameter = 81 nm AuNPs), where y and x are the LSPR λ_{max} shifts of the single AuNP and analyte (PSA–ACT complex) concentration (ng/ml), respectively. The error bars in Fig. 4 illustrate the relative standard deviation for four replicates ($n = 4$). Based on these equations, the expected shift for different PSA concentrations can be estimated. As shown in Fig. 4, the linear dynamic range of individual AuNPs with a diameter of approximately 21 nm was from 10^{-4} to 10^{-1} ng/ml, and in the case of the plasmonic responses of individual AuNPs with approximate diameters of 43 and 81 nm, the linear dynamic ranges were from 10^{-3} to 10^{0} ng/ml and from 10^{-2} to 10^{1} ng/ml, respectively. Thus, the total linear dynamic range was obtained at a concentration range from 10^{-4} to 10^{1} ng/ml. From these results, it can be concluded that the size of the nanoparticles strongly affects the LSPR sensitivity, the linear dynamic range, and the LSPR behavior of the individual spherical Au nanosensor. The smaller nanoparticles show higher LSPR sensitivity because their smaller surface area reduces nonspecific binding and enables more targeted binding on the AuNP surface. Moreover, the smaller nanoparticles produce more confined electromagnetic fields; thus, they are more sensitive to single molecules, which occupy a greater portion of the sensing volume. However, the nanoparticles less than 20 nm in diameter are very hard to visualize by a dark-field microscope [38]. Hence, nanoparticle size should be carefully chosen to ensure sufficient signal intensity for LSPR assays. Furthermore, the smaller nanoparticles show smaller values for the saturation response owing to the smaller surface area for surface coverage of the nanoparticle. As a result, the maximum number of protein molecules conjugated to the surface of AuNPs is reduced. Thus, it can be concluded that the dynamic range of detection was dependent on the nanoparticle size.

To detect specific protein biomarkers more accurately, as well as to verify the limit of detection, it is essential to examine the interaction between nontarget proteins and sensing materials because unexpected binding events can generate noise leading to aberrance of quantitative analysis of biomolecular recognition. Therefore, nonspecific binding tests were performed with several common proteins in human serum such as BSA, fibrinogen, and IgG. As shown in Fig. 5, after the nontarget proteins (0.1 ng/ml) were injected over the anti-PSA functionalized AuNP surface in the flow cell, the plasmonic responses of these proteins increased only slightly below 1.0 nm. The low nonspecific binding of these proteins could be explained due to all of the unreacted sites on the surface of the functionalized AuNPs being effectively deactivated by the ethanolamine injected over the particle surface. Compared with the LSPR λ_{max} shifts from the specific interaction between conjugated PSA mAb and PSA–ACT, the nonspecific binding events of the undesired proteins were negligible even at very high concentrations. Thus, the target protein, the PSA–ACT complex, can be specifically detected using single AuNP sensors. From these results, it can be concluded that the detection limit of the individual spherical Au nanosensor with a diameter of approximately 21 nm was approximately 0.1 pg/ml, corresponding to the LSPR λ_{max} shift of approximately 2.95 nm. This detection limit can be compared with the values obtained from the well-known assays based on barcode DNA [39]. Compared with all detection limits of commercial tests for PSA detection (0.05–0.005 ng/ml) and other formats such as surface plasmon resonance (0.15–18.1 ng/ml), surface plasmon fluorescence spectroscopy (3 pg/ml), and immuno-PCR (0.1 pg/ml) [40], the detection platform based on individual spherical Au nanosensors is ultrasensitive. These results indicate that this approach suggests possibilities for the future about using single AuNPs with various sizes as a label-free biosensor to quantitatively detect a lot of disease-related proteins in a wide concentration range.

Conclusions

We have demonstrated that the plasmonic responses of single AuNPs with various sizes can be used for analysis of biorecognition. The plasmonic responses of single AuNPs were measured as the shift value of LSPR maximum wavelength of each single AuNP using a dark-field microspectroscopy system. The relationship between particle size and plasmonic response induced by the binding of the adsorbates and target analytes was described by the comparative analysis of the resonant Rayleigh light scattering spectra of each single AuNP. In addition, the linear dynamic range of each plasmonic response corresponding to the binding of the

PSA–ACT complex with a wide concentration range was determined by the calibration curves using single AuNPs with various sizes as a biosensor. Consequently, the total linear dynamic range was obtained in the concentration range of 10^{-4} to 10 ng/ml, with the smallest detectable concentration at 0.1 pg/ml being determined with an LSPR λ_{max} shift of approximately 2.95 nm. This result shows that this approach can provide a highly sensitive and wide-ranging analytical method for detecting not only protein biomarkers but also other biological interactions. Moreover, the unique plasmonic property of each single nanoparticle can contribute to the development of the biosensing platform, allowing fast, simultaneous, economical, and label-free detection of multiple analytes.

Acknowledgments

This work was supported by the Korea Science and Engineering Foundation (KOSEF) National Research Laboratory (NRL) Program (R0A-2008-000-20078-0), the Basic Science Research Program (2010-0027771), and a grant from the Carbon Dioxide Reduction & Sequestration Research Center (DG2-201), one of the 21st Century Frontier Programs funded by the Ministry of Science and Technology of the Korean government of the Republic of Korea.

References

[1] R.G. Freeman, K.C. Grabar, K.J. Allison, R.M. Bright, J.A. Davis, A.P. Guthrie, M.B. Hommer, M.A. Jackson, P.C. Smith, D.G. Walter, M.J. Natan, Self-assembled metal colloid monolayers: an approach to SERS substrates, Science 267 (1995) 1629–1632.
[2] M. Kahl, E. Voges, S. Kostrewa, C. Viets, W. Hill, Periodically structured metallic substrates for SERS, Sens. Actuat. B 51 (1998) 285–291.
[3] C.L. Haynes, R.P. Van Duyne, Plasmon-sampled surface-enhanced Raman excitation spectroscopy, J. Phys. Chem. B 107 (2003) 7426–7433.
[4] E.C. Hao, G.C. Schatz, R.C. Johnson, J.T. Hupp, Hyper-Rayleigh scattering from silver nanoparticles, J. Chem. Phys. 117 (2002) 5963–5966.
[5] A. Podlipensky, J. Lange, G. Seifert, H. Graener, I. Cravetchi, Second-harmonic generation from ellipsoidal silver nanoparticles embedded in silica glass, Opt. Lett. 28 (2003) 716–718.
[6] C.K. Chen, T.F. Heinz, D. Richard, Y.R. Shen, Surface-enhanced second-harmonic generation and Raman scattering, Phys. Rev. B 27 (1983) 1965–1979.
[7] A.M. Moran, J. Sung, E.M. Hicks, R.P. Van Duyne, K.G. Spears, Second harmonic excitation spectroscopy of silver nanoparticle arrays, J. Phys. Chem. B 109 (2005) 4501–4506.
[8] C. Cao, S.J. Sim, Signal enhancement of surface plasmon resonance immunoassay using enzyme precipitation-functionalized gold nanoparticles: a femto-molar level measurement of anti-glutamic acid decarboxylase antibody, Biosens. Bioelectron. 22 (2007) 1874–1880.
[9] N. Nath, A. Chilkoti, A colorimetric gold nanoparticle sensor to interrogate biomolecular interactions in real time on a surface, Anal. Chem. 74 (2002) 504–509.
[10] F. Frederix, J. Friedt, K. Choi, W. Laureyn, A. Campitelli, D. Mondelaers, G. Maes, G. Borghs, Biosensing based on light absorption of nanoscaled gold and silver particles, Anal. Chem. 75 (2003) 6894–6900.
[11] M. Lahav, A. Vaskevich, I. Rubinstein, Biological sensing using transmission surface plasmon resonance spectroscopy, Langmuir 20 (2004) 7365–7367.
[12] A.J. Haes, W.P. Hall, L. Chang, W.L. Klein, R.P. Van Duyne, A localized surface plasmon resonance biosensor: first steps toward an assay for Alzheimer's disease, Nano Lett. 4 (2004) 1029–1034.
[13] T. Endo, K. Kerman, N. Nagatani, Y. Takamura, E. Tamiya, Label-free detection of peptide nucleic acid–DNA hybridization using localized surface plasmon resonance based optical biosensor, Anal. Chem. 77 (2005) 6976–6984.
[14] T.R. Jensen, M. Duval Malinsky, C.L. Haynes, R.P. Van Duyne, Nanosphere lithography: tunable localized surface plasmon resonance spectra of silver nanoparticles, J. Phys. Chem. B 104 (2000) 10549–10556.
[15] A.D. McFarland, R.P. Van Duyne, Single silver nanoparticles as real-time optical sensors with zeptomole sensitivity, Nano Lett. 3 (2003) 1057–1062.
[16] G. Mie, Beiträge zur Optik trüber Medien, speziell kolloidaler Metallösungen, Ann. Phys. 25 (1908) 377–445.
[17] J.J. Mock, M. Barbic, D.R. Smith, D.A. Schultz, S. Schultz, Shape effects in plasmon resonance of individual colloidal silver nanoparticles, J. Chem. Phys. 116 (2002) 6755–6759.
[18] L.J. Sherry, S.-H. Chang, G.C. Schatz, R.P. Van Duyne, B.J. Wiley, Y. Xia, Localized surface plasmon resonance spectroscopy of single silver nanocubes, Nano Lett. 5 (2005) 2034–2038.
[19] C.L. Nehl, N.K. Grady, G.P. Goodrich, F. Tam, N.J. Halas, J.H. Hafner, Scattering spectra of single gold nanoshells, Nano Lett. 4 (2004) 2355–2359.
[20] C.J. Orendorff, T.K. Sau, C.J. Murphy, Shape-dependent plasmon-resonant gold nanoparticles, Small 2 (2006) 636–639.
[21] J. Prikulis, F. Svedberg, M. Käll, J. Enger, K. Ramser, M. Goksör, D. Hanstorp, Optical spectroscopy of single trapped metal nanoparticles in solution, Nano Lett. 4 (2004) 115–118.
[22] J.J. Mock, D.R. Smith, S. Schultz, Local refractive index dependence of plasmon resonance spectra from individual nanoparticles, Nano Lett. 3 (2003) 485–491.
[23] L.J. Sherry, R. Jin, C.A. Mirkin, G.C. Schatz, R.P. Van Duyne, Localized surface plasmon resonance spectroscopy of single silver triangular nanoprisms, Nano Lett. 6 (2006) 2060–2065.
[24] C. Sönnichsen, S. Geier, N.E. Hecker, G. von Plessen, J. Feldmann, H. Ditlbacher, B. Lamprecht, J.R. Krenn, F.R. Aussenegg, V.Z.H. Chan, J.P. Spatz, M. Moller, Spectroscopy of single metallic nanoparticles using total internal reflection microscopy, Appl. Phys. Lett. 77 (2000) 2949–2951.
[25] G.J. Nusz, S.M. Marinakos, A.C. Curry, A. Dahlin, F. Hook, A. Wax, A. Chilkoti, Label-free plasmonic detection of biomolecular binding by a single gold nanorod, Anal. Chem. 80 (2008) 984–989.
[26] C. Cao, S.J. Sim, Resonant Rayleigh light scattering response of individual Au nanoparticles to antigen–antibody interaction, Lab Chip 9 (2009) 1836–1839.
[27] P.L. Truong, C. Cao, S. Park, M. Kim, S.J. Sim, New method for non-labeling attomolar detection of diseases based on individual gold nanorod immunosensor, Lab Chip 11 (2011) 2591–2597.
[28] U. Kreibig, M. Vollmer, Optical Properties of Metal Clusters, Springer, Berlin, 1995.
[29] Y. Choi, Y. Park, T. Kang, L.P. Lee, Selective and sensitive detection of metal ions by plasmonic resonance energy transfer-based nanospectroscopy, Nat. Nanotechnol. 4 (2009) 742–746.
[30] G.L. Liu, Y.-T. Long, Y. Choi, T. Kang, L.P. Lee, Quantized plasmon quenching dips nanospectroscopy via plasmon resonance energy transfer, Nat. Methods 4 (2007) 1015–1017.
[31] H. Li, J. Huang, J. Lv, H. An, X. Zhang, Z. Zhang, C. Fan, J. Hu, Nanoparticle PCR: nanogold-assisted PCR with enhanced specificity, Angew. Chem. Int. Ed. 44 (2005) 5100–5103.
[32] K.R. Brown, M.J. Natan, Hydroxylamine seeding of colloidal Au nanoparticles in solution and on surfaces, Langmuir 14 (1998) 726–728.
[33] G. Chumanov, K. Sokolov, B.W. Gregory, T.M. Cotton, Colloidal metal films as a substrate for surface-enhanced spectroscopy, J. Phys. Chem. 99 (1995) 9466–9471.
[34] P. Ghosh, G. Han, M. De, C.K. Kim, V.M. Rotello, Gold nanoparticles in delivery applications, Adv. Drug Deliv. Rev. 60 (2008) 1307–1315.
[35] K.H. Su, Q.H. Wei, X. Zhang, J.J. Mock, D.R. Smith, S. Schultz, Interparticle coupling effects on plasmon resonances of nanogold particles, Nano Lett. 3 (2003) 1087–1090.
[36] W. Rechberger, A. Hohenau, A. Leitner, J.R. Krenn, B. Lamprecht, F.R. Aussenegg, Optical properties of two interacting gold nanoparticles, Opt. Commun. 220 (2003) 137–141.
[37] C. Sönnichsen, T. Franzl, T. Wilk, G. Von Plessen, J. Feldmann, Plasmon resonances in large noble-metal clusters, New J. Phys. 4 (2002) 93.1–93.8.
[38] J.N. Anker, W.P. Hall, O. Lyandres, N.C. Shah, J. Zhao, R.P. Van Duyne, Biosensing with plasmonic nanosensors, Nat. Mater. 7 (2008) 442–453.
[39] J.M. Nam, C.S. Thaxton, C.A. Mirkin, Nanoparticle-based bio-bar codes for the ultrasensitive detection of proteins, Science 301 (2003) 1884–1886.
[40] D.A. Healy, C.J. Hayes, P. Leonard, L. McKenna, R. O'Kennedy, Biosensor developments: application to prostate-specific antigen detection, Trends Biotechnol. 25 (2007) 125–131.